1982

A study of the bottom boundary layer over the Eastward Scarp of the Bermuda Rise

Arlene A. Bird

Georges L. Weatherly

See next page for additional authors

Citation/Publisher Attribution
Bird, A. A., Weatherly, G. L., and Wimbush, M. (1982), A study of the bottom boundary layer over the Eastward Scarp of the Bermuda Rise, *J. Geophys. Res.*, 87(C10), 7941– 7954, doi: 10.1029/JC087iC10p07941.
Available at: https://doi.org/10.1029/JC087iC10p07941

JOURNAL OF GEOPHYSICAL RESEARCH, VOL. 87, NO. C10, PAGES 7941–7954, SEPTEMBER 20, 1982

A Study of the Bottom Boundary Layer Over the Eastward Scarp of the Bermuda Rise

ARLENE A. BIRD[1] AND GEORGES L. WEATHERLY

Department of Oceanography, The Florida State University, Tallahassee, Florida 32306

MARK WIMBUSH

Graduate School of Oceanography, University of Rhode Island, Kingston, Rhode Island 02881

Velocity and temperature measurements from the bottom boundary layer (BBL) over the Eastward Scarp of the Bermuda Rise in water depth of 4620 m show little variability over an 8-month period. The free-stream flow 62 m above the bottom was south-southeasterly following the isobaths in the region with an average speed of 22 cm/s. The current vector in the BBL rotated an average of 5° in a counterclockwise sense between 62 and 0.8 m above the bottom. The thickness of the BBL was ~40 m and the average magnitude of the bottom stress was ~0.7 dynes/cm^2. Mean speed profiles, height of the BBL, and the magnitude of the bottom stress predicted by a model compare favorably with the observations, but the model predicts a rotation of the current vector between 62 and 0.8 m more than twice that measured. The time-dependent nature of the flow field is also reproduced by the model. The Bermuda Rise data and speed profile measurements at the base of the Scotian Rise show that the M_2 clockwise polarized tide is damped more than the mean current as the bottom is approached in the BBL. This phenomenon is reproduced by the model and can be explained by differing effective Ekman layer thicknesses associated with tidal and steady components of the flow.

1. INTRODUCTION

This study was undertaken for two purposes. The first was to examine an 8-month near-bottom velocity and temperature record from the Eastward Scarp of the Bermuda Rise at 32°52.5'N, 57°29.0'W in water depth of 4620 m, and to compare these observations with a numerical bottom boundary layer (BBL) model described by *Weatherly et al.* [1980] and *Weatherly and Martin* [1978]. Simulations of the BBL with the parameters at this site are used to explore the effects of a sloping bottom, density stratification, tidal oscillations, and unsteady free-stream flow on the structure and dynamics of the boundary layer. The second purpose was to extend the study begun in *Weatherly et al.* [1980] of the combined effects of tidal and mean currents on the structure of the BBL. It has been observed in flows composed of a mean flow and a small oscillatory flow that these components are damped unequally as the bottom is approached in the BBL [*Weatherly and Van Leer,* 1977; *Weatherly and Wimbush,* 1980]. The model reproduces this feature, and a mechanism is presented.

2. REVIEW OF THEORY AND LITERATURE

The equations used in this study of the BBL are

$$\frac{\partial U}{\partial t} - fV = \frac{\partial}{\partial z}(\overline{-u'w'}) + \alpha'\lambda\theta \tag{1a}$$

$$\frac{\partial V}{\partial t} + fU = \frac{\partial}{\partial z}(\overline{-v'w'}) \tag{1b}$$

$$\frac{\partial \theta}{\partial t} + \alpha\frac{\partial(\theta_I)U}{\partial z} = \frac{\partial}{\partial z}(\overline{-\theta'w'}) \tag{2}$$

Here U and V are the x and y components of velocity relative to the geostrophic velocity components, U_I and V_I, in the interior above the boundary layer, and z is the vertical coordinate, positive upward from the bottom; α' is the bottom slope and α is the isotherm slope relative to the bottom, both assumed to be uniform and small and tilted in the x direction only; f is the Coriolis parameter and $\lambda = \beta g$ is a buoyancy parameter, where β is the coefficient of thermal expansion for seawater; θ is the potential temperature relative to the interior, or free-stream temperature, θ_I linearly extrapolated into the BBL. Because of the linearity of the θ-S relation, all variations in the density field may be taken into account by the heat equation alone.

$\partial(\theta_I)/\partial z$ is taken to be constant and set to match the Brunt-Vaisala frequency in the interior; $\overline{-u'w'}$ and $\overline{-v'w'}$ are turbulent Reynolds stresses divided by density, and $\overline{-\theta'w'}$ is the turbulent heat flux divided by density and heat capacity.

The boundary conditions are

$$\begin{aligned}
&\text{At } z = z_0 \\
&\qquad U = -U_I \\
&\qquad V = -V_I \\
&\qquad \frac{\partial \theta}{\partial z} = -\frac{\partial(\theta_I)}{\partial z} \\
&\text{As } z \to \infty \\
&\qquad U \to 0 \quad \overline{-u'w'} \to 0 \\
&\qquad V \to 0 \quad \overline{-v'w'} \to 0 \\
&\qquad \theta \to 0 \quad \overline{-\theta'w'} \to 0
\end{aligned} \tag{4}$$

where z_0 is the roughness parameter.

At the ocean bottom, z_0, a no-slip condition is imposed on the velocity, and there is no heat flux through the ocean floor. Above the BBL, the velocity is in geostrophic balance, the temperature is the interior temperature θ_I, and the

[1] Now at Department of Oceanography, Naval Postgraduate School, Monterey, California 93940.

Paper number 2C0682.
0148-0227/82/002C-0682$5.00

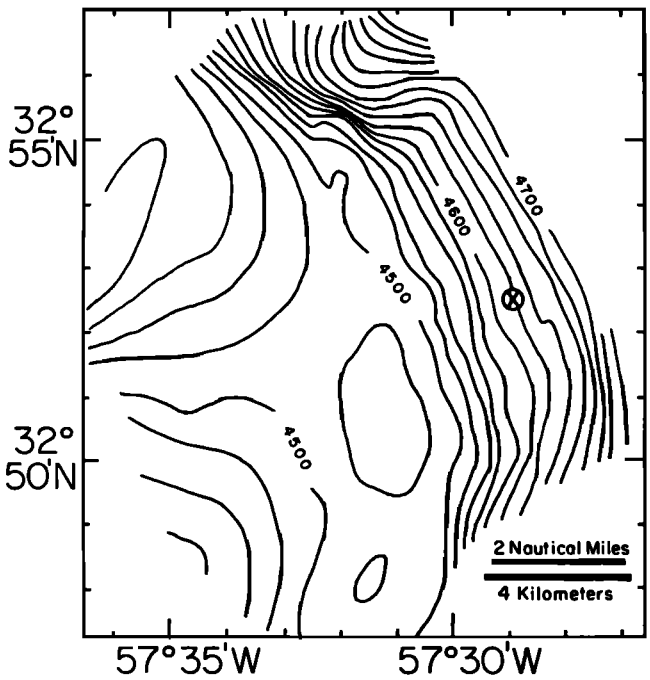

Fig. 1. Topographic map of the Eastward Scarp of the Bermuda Rise [from *Lonsdale*, 1978]. Site of observations is indicated by cross. Depths are in meters.

turbulent fluxes of momentum and heat vanish. For further discussion of the system of equations and boundary conditions as well as discussion of the second-order closure scheme used, see *Weatherly and Martin* [1978].

The thickness of a turbulent Ekman layer formed in a neutrally stratified fluid in a steady flow may be written

$$h = cu_*/f \tag{5}$$

where c is a constant usually taken to be von Karman's constant k and u_* is the friction velocity defined as

$$u_* = (|\vec{\tau_0}|/\rho)^{1/2} \tag{6}$$

where $\vec{\tau_0}$ is the bottom stress and ρ is the fluid density. This expression represents the height at which the velocity is 99% of its geostrophic value [*Caldwell et al.*, 1972]. In a stably stratified fluid, buoyancy effects inhibit turbulence, confining the velocity shear to a thinner layer. An expression that incorporates the stratification of the fluid is

$$h = 1.3u_*/[f(1 + N_0^2/f^2)^{1/4}] \tag{7}$$

where N_0 is the Brunt-Vaisala frequency in the interior [*Weatherly and Martin*, 1978]. This layer thickness represents the height at which the Richardson number first becomes ≥ 0.21. In the few studies of deep oceanic bottom boundary layers, thicknesses of the order of 20–30 m have been observed [*Bowden*, 1978].

The bottom stress $\vec{\tau_0}$ may be computed by vertical integration of the horizontal momentum equations

$$\int_0^h \frac{\partial U}{\partial t}\,dz - f\int_0^h V\,dz = -\frac{\tau_0^x}{\rho} + \alpha'\lambda\int_0^h \theta\,dz \tag{8a}$$

$$\int_0^h \frac{\partial U}{\partial t}\,dz + f\int_0^h U\,dz = \frac{\tau_0^y}{\rho} \tag{8b}$$

where $\vec{\tau_0} = (\tau_0^x, \tau_0^y)$. In (8) the stresses are taken to be zero at $z = h$. *Mercado and Van Leer* [1976], using cyclosonde profile data, estimated $\vec{\tau_0}$ by using (8) neglecting the time-dependent and sloping bottom terms.

The friction velocity defined by (6) is an important scaling parameter for turbulent boundary layers. For the BBL it is a function of $|\vec{V}_l|$, f, z_0, and N_0. *Weatherly and Martin* [1978] argue that for values of N_0 typical of the ocean, the dependence of u_* on N_0 is very weak. Thus, using similarity expressions given in *Csanady* [1967], *Blackadar and Tennekes* [1968], and values of surface Rossby number typical of the deep ocean, u_* can be estimated as 3–5% of the geostrophic speed. Further discussion of the dependence of u_* on stratification may be found in *Bird* [1981].

The total veering angle, α_0, is also a function of surface Rossby number [*Csanady*, 1967] and N_0 [*Bird*, 1981], with values of 10° to 20° expected for surface Rossby numbers and values of N_0 typical of the deep ocean. In the lowest part of the BBL, the logarithmic layer, the current vector is not expected to turn appreciably with depth because Coriolis effects are negligible there. *Kundu* [1976] reported an Ekman veering angle of 6° between 5 and 20 m above the ocean bottom on the Oregon shelf, well above the logarithmic layer (~3 m) thick. The current veered counterclockwise (CCW) as the bottom was approached, as expected in the northern hemisphere. *Weatherly* [1972], in a study of the BBL beneath the Florida Current, observed a mean veering of

TABLE 1. Means and Standard Deviations for the Velocity Components, Speed, Direction, and Temperature at the Four Current Meter Sites for the Entire Data Set

	U	V	Speed	Direction	Temperature
62 m					
Mean	4.77	−21.02	21.81	167.39	2.22
Standard deviation	3.48	4.84	4.94	9.12	0.02
12 m					
Mean	5.72	−19.29	20.35	163.68	2.21
Standard deviation	3.27	4.15	4.30	8.98	0.02
6.9 m					
Mean	5.94	−17.98	19.19	161.78	2.22
Standard deviation	3.23	4.06	4.15	9.65	0.02
0.8 m					
Mean	3.92	−12.98	13.70	163.33	2.22
Standard deviation	2.08	2.77	2.85	8.61	0.02

The velocity components and speeds are in units of cm/s, direction is degrees from true north, and the temperature is the in situ temperature in °C.

10°CCW in the lowest 3 m and no mean veering above the logarithmic layer over a period of 6 days. Veering above the logarithmic layer was observed only when the current was very strong (~30 cm/s). It was suggested that the variability in direction of the current due to the presence of a strong diurnal tide prevented the Ekman layer from forming above the logarithmic layer. In a study of the BBL in the eastern tropical North Pacific, a mean veering of 11° CCW was observed between 50 and 8 m above the bottom, but between 8 and 4 m, the current vector turned 6° in a clockwise sense [*Hayes*, 1980]. Hayes attributes this clockwise rotation to small-scale topography near the mooring; the discrepancy is too large to be explained by an instrumental effect.

3. Bermuda Rise Data

An 8-month long time series of current speed, direction, and temperature was obtained from the BBL on the Eastward Scarp of the Bermuda Rise at 32°52.5'N, 57°29.0'W. Four vector averaging current meters (VACMs) were positioned at 0.8, 6.9, 12, and 62 m above the bottom from September 1978 through April 1979. The terrain slopes upward toward the west-southwest at approximately 35 m per kilometer (see Figure 1). Although the small-scale topography is not known at the mooring site, a deep-tow survey on the Eastward Scarp determined that there are furrows about 6 km upstream [*McCave et al.*, 1982].

In the vertical, the VACMs span the entire BBL, providing needed information on veering and speed profiles. The flow measured by each current meter was strong during the entire experiment, giving a good signal-to-noise ratio. There are several shortcomings of the data set, however; there is a large gap in the moored array between 12 and 62 m above the bottom, the roughness parameter is unknown, and the slope of the isopycnal or isothermal surfaces relative to the bottom is not known either from historical or hydrographic data. Also, the location at 32°52.5'N places the inertial frequency

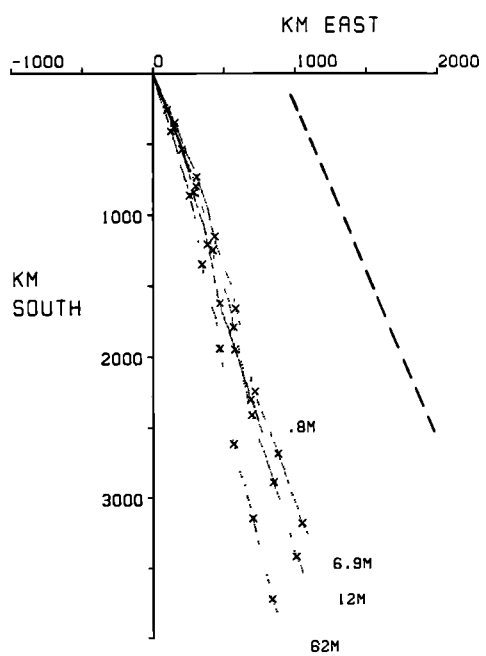

Fig. 2. Progressive vector diagrams of the Bermuda Rise data. Each point represents a 1-day average; cross denotes the beginning of a monthly interval. The dashed line represents the orientation of the isobaths at the mooring site.

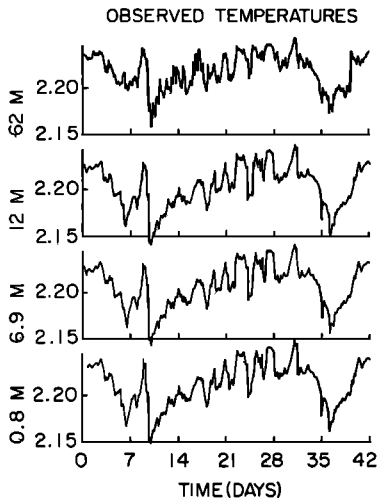

Fig. 3. In situ 2-hour averaged temperature (°C) for the first 6 weeks of the experiment.

near the K1 and O1 tidal frequencies so that these signals are difficult to separate.

The flow in the BBL at this location was strong and remarkably steady in direction for the duration of the study. The free-stream flow 62 m above the bottom was south-southeasterly (167° from north), following the isobaths in the region, with an average speed of 22 cm/s. Table 1 summarizes means and variances for the entire record of 2-hour averages at each level for the velocity components u and v, speed, direction, and temperature. Progressive vector diagrams for the four current meters using daily averages of the velocities are plotted in Figure 2. Although the flow is extremely steady with time, flows in this area of the North Atlantic may vary considerably on relatively short spatial scales [*Schmitz*, 1980]. In contrast to the Bermuda Rise data, Schmitz's two current meters closest to the Bermuda Rise (at 31.5°N, 55.0°W and at 35.0°N, 55.0°W) each measured a very weak mean flow (~1 cm/s at 4000 m depth) directed approximately eastward.

The average measured veering between 62 and 6.9 m above the bottom was 6° in a counterclockwise sense. Between the two current meters at 6.9 and 0.8 m, a mean veering of 1.5° was observed over the entire record, but it was in a clockwise sense. The rms accuracy of the direction for a VACM is estimated to be 2.0° [*Bryden*, 1976], so that this small veering may have been an instrumental effect. Furthermore, the vane of the current meter nearest to the ocean floor was between the legs of the tripod, and wakes shed by the legs may have offset its orientation. Near the end, the veering became slightly positive (CCW). Within the accuracy of the instrument, however, there was no significant veering in the lowest 6.9 m of the BBL, consistent with theory.

A mixed layer depth typically greater than 12 m but less than 62 m may be inferred from the temperature data. Inspection of a portion of the temperature record (Figure 3) shows such good coherence between the lowest three sensors that they must have been in the bottom mixed layer. The differences in temperature between the lowest three sensors were nearly constant in time, while the difference between at 62 and 0.8 m was highly variable (Figure 4). Cross-spectral analysis between the temperature at 12 m and

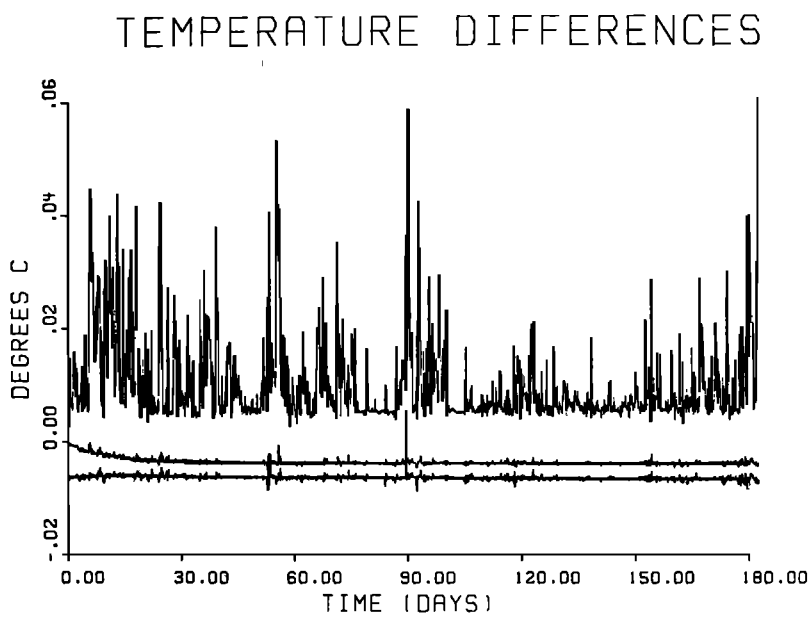

Fig. 4. Temperature time series at 6.9 m, 12 m, and 62 m relative to the temperatures measured at 0.8 m above the bottom.

at 0.8 m shows almost perfect coherence and no phase difference except at high frequencies (Figure 5*a*). The cross spectrum between the time series at 62 and 12 m shows less coherence and nonzero phase angles (Figure 5*b*). At times, however, such as the end of day 2 of the record (Figure 9*a*), the mixed layer may have extended to 62 m.

Another estimate of boundary layer thickness may be made by using equation (5). Estimating u_* as 4% of the mean speed at 62.0 m, taking $c = 0.4$ and using the appropriate f for this latitude, h is inferred to be 44 m. If the stratification of the water column is taken into account by using equation (7), $h = 41$ m. The Brunt-Vaisala frequency was determined to be 7×10^{-5} s^{-1} from potential temperature profiles made at the time the VACMs were deployed and use of the potential temperature-salinity relation for the region [*Worthington and Metcalf*, 1961].

Oceanic flow in the BBL may be decomposed into a steady current and an oscillatory current. The oscillatory current can be further resolved into a clockwise polarized flow and a counterclockwise polarized flow by means of rotary spectral analysis. Table 2 summarizes the results of the rotary spectral analysis using three-band smoothing. The oscillations were dominated by the M_2 tidal component, the principal lunar semi-diurnal tide, which has a period of 12.4 hours. At this latitude, the inertial period (22.1 hours) is so close to those of the diurnal tidal components K_1, the lunisolar (23.9 hours), and O_1, the principal lunar (25.8 hours), that their contributions are not easily separable. Rotary and autospectral analyses indicate that the energy of the inertial motions was greater than that of the diurnal tidal components. Note in Table 2 that the clockwise polarized components have higher amplitudes than the corresponding counterclockwise polarized components.

The stress on the ocean floor, an important parameter in studies of erosion and sediment transport, may be estimated by vertical integration of the momentum equations through the BBL by using equations (8*a*, *b*). The slope term in the x momentum equation cannot be estimated with the data

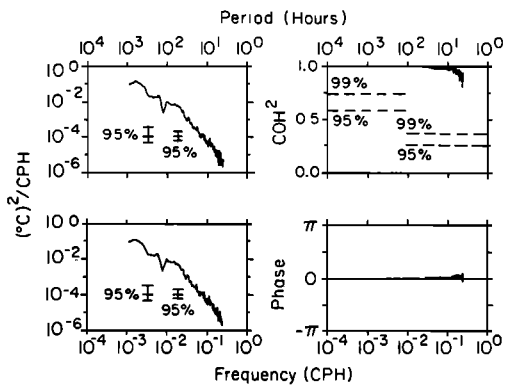

Fig. 5*a*

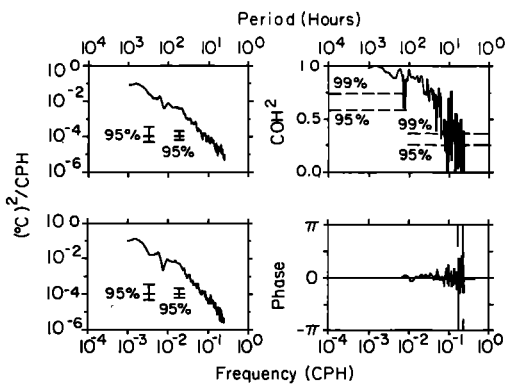

Fig. 5*b*

Fig. 5. (*a*) Starting from lower left and proceeding clockwise: autospectrum of temperature 0.8 m, autospectrum of temperature at 12 m, coherency squared of cross spectra, and phase of cross spectra. For frequencies <0.01 cph smoothing over three band widths and for frequencies >0.01 cph smoothing over 20 band widths. For positive phase higher record leads lower record. Phase is drawn only if coherency squared ≥0.5. (*b*) As in Figure 5*a* except temperature time series at 12 m and 62 m.

TABLE 2. Amplitudes of Tidal Components in cm/s Determined from Rotary Spectral Analysis.

	0.8 m	6.9 m	12 m	62 m
M_2+	0.730	1.150	1.198	1.352
Inertial, K_1+, and O_1+	0.369	0.548	0.570	0.674
M_2-	0.344	0.523	0.546	0.542
K_1- and O_1-	0.227	0.345	0.346	0.376

Plus denotes clockwise polarization; minus, counterclockwise polarization.

available. Inclusion of this term would have the effect of decreasing the x component of the bottom stress, making the angle between $\vec{V}_I$ and $\vec{\tau_0}$ smaller.

To estimate $\vec{\tau_0}$ from the velocity data, the integrals were evaluated by using the trapezoidal rule. In a coordinate system in which the free-stream velocity is aligned along the negative y axis, and taking the top of the boundary layer h to be 62 m, this procedure yields a magnitude of the bottom stress $|\vec{\tau_0}|$ equal to 0.7 dynes/cm^2 directed at an angle 31.6° counterclockwise from $\vec{V}_I$. From estimates of the thickness of the boundary layer, however, h is of the order of 40 m. Therefore, if a data point is included in the computation at 40 m above the bottom having the same velocity as at 62 m, integration using the trapezoidal rule yields $|\vec{\tau_0}| = 0.7$ dynes/cm^2 and a direction of 65.2° counterclockwise from $\vec{V}_I$. Another estimate of the bottom stress was obtained by fitting exponential curves to the data and integrating these functions analytically. For $h = 62.0$ m, this procedures gives $|\vec{\tau_0}| = 0.6$ dynes/cm^2 directed 54.2° counterclockwise from $\vec{V}_I$. For $h = 40$ m, this method yields $|\vec{\tau_0}| = 1.1$ dynes/cm^2 directed 76.8 from $\vec{V}_I$.

The direction of the computed stress is probably greatly in error due in part to the uncertainty caused by the lack of data between 12 and 62 m and in part to the omission of the sloping term. Inclusion of the latter could decrease the x component of the stress by as much as 0.3 dynes/cm^2, causing the stress to be much closer in direction to $\vec{V}_I$. For example, for the exponential fit calculation with $h = 62$ m, the magnitude of the bottom stress would be reduced 36%, and the direction from $\vec{V}_I$ would be reduced 59% to 22.4°. The estimates of the magnitude of the bottom stress compare favorably with the value of 0.78 dynes/cm^2 computed by using equation (5) and the value of u_* determined earlier by a drag law.

4. Model Results and Comparison to Data

In this section, results of simulations of the Bermuda Rise BBL using the model described in *Weatherly and Martin* [1978] are presented. Input parameters for this numerical model are the Coriolis parameter, the free-stream velocity, assumed to be dependent only on time, the stratification of the water column, the roughness parameter, the slope of the bottom, and the slope of the isopycnals relative to the bottom slope. All of these parameters are known at this location except the roughness parameter z_0 and the slope of the isopycnals relative to the bottom slope α. The roughness parameter z_0 is taken to be 0.03 cm for definiteness: The results of the model are not very sensitive to the choice of z_0 [*Weatherly and Martin*, 1978]. A range of probable values of z_0 can be found by solving the logarithmic relation for current speed $u(z) = (u_*/k)\ln(z/z_0)$ at $z = 0.8$ m. Since u_* is 3 to 5% of $|\vec{V}_I|$, solving for z_0 gives a lower bound of 0.001 cm and an upper bound of 0.173 cm. The value of z_0 used in the model simulations, 0.03 cm, is well within this range.

Although the bottom slope α' used in the x momentum equation (1a) was determined from the topographic map (Figure 1), the isopycnal slope relative to the bottom, α, used in the heat equation (2) could not be determined from the hydrographic data available or from historical data. Three situations with differing values of α were simulated: $\alpha = 0$, 0.01, and 0.035. The first case, $\alpha = 0$, represents isopycnals parallel to the bottom; the second simulates the case where the isopycnals intersect the bottom at an angle less than the bottom slope; the third represents level isopycnals over an inclined bottom.

The model solves the one-dimensional momentum and heat equations for the BBL (1) and (2) subject to boundary conditions (4). The model determines profiles of velocity, eddy diffusivity for momentum and heat, the turbulent kinetic energy, temperature, density, Richardson number, and veering angle at every time step. The model also computes the bottom stress and friction velocity at each time step.

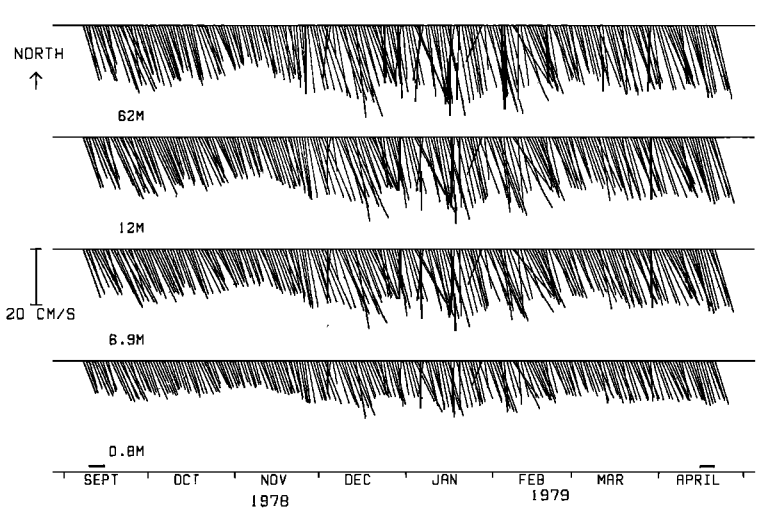

Fig. 6. Stick plot of daily averaged Bermuda Rise data. Horizontal bar over "September" shows time interval considered here. Horizontal bar over "April" shows time interval considered in Bird (1981) but not here. Note the counterclockwise rotation with decreasing height above bottom between 62 m and 6.9 m.

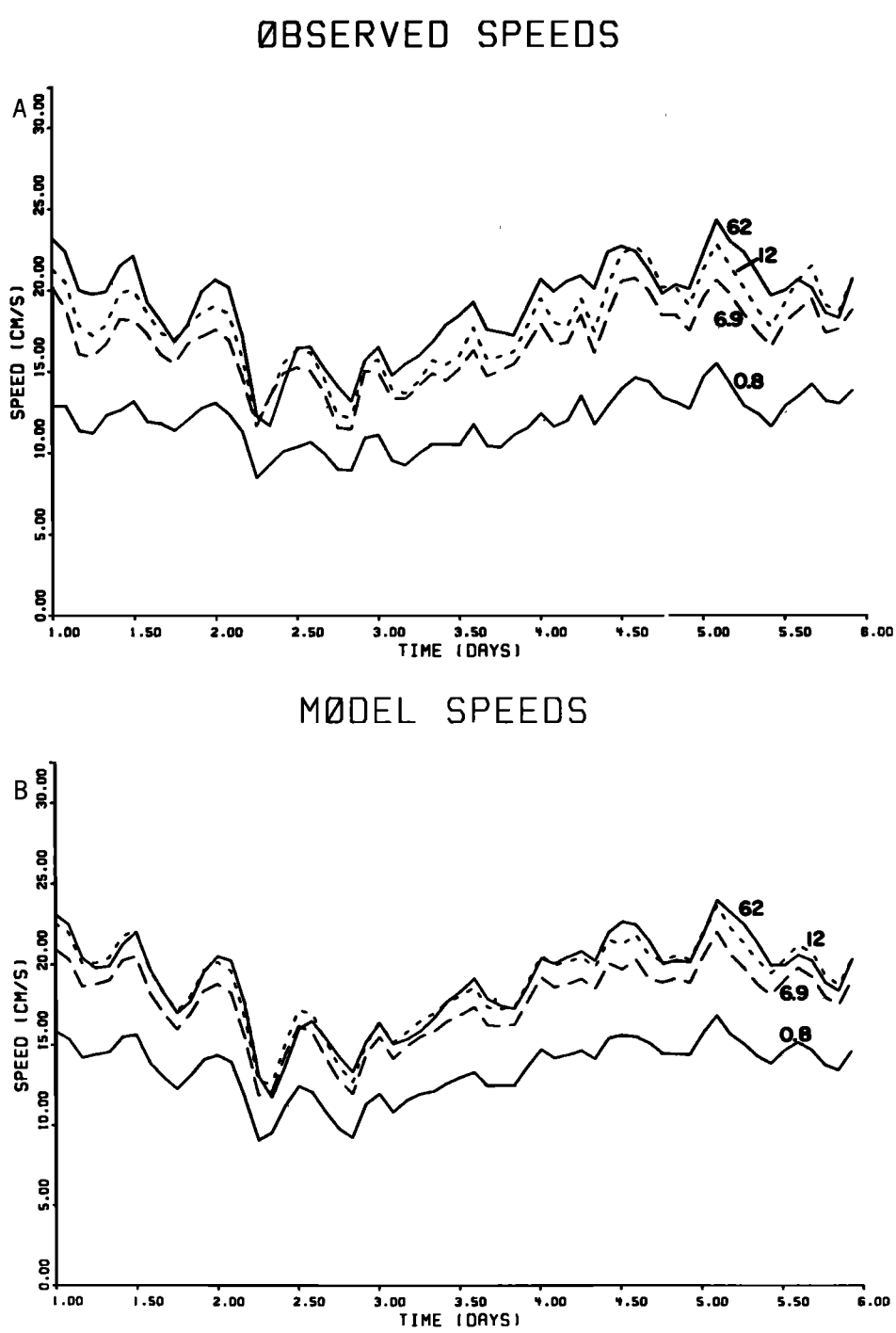

Fig. 7. (Top) Observed speeds and (bottom) model speed predictions.

Two 5-day sections of the data were chosen for comparison with model simulations. Five days is long enough to make direct comparisons between model and data but not so long as to be prohibitively expensive in computer time. The two 5-day intervals chosen are indicated on a stick plot of the entire time series in Figure 6. The first section will be analyzed and discussed here; analysis of the second section led to similar conclusions [*Bird*, 1981]. The first 5-day sample from the observations starts 1 day after the record begins; this 5-day section was chosen because it was closest in time to a deep-tow survey, from which the stratification was derived. Time series of observed speeds, direction, veering and temperature are plotted in Figures 7*a*, 8*a*, and 9*a*.

To gain insight into the processes determining the structure and dynamics of the BBL, the simulations proceeded in stages. First, the mean features of the 5-day period were simulated with a steady free-stream velocity which was obtained by averaging the velocity at 62 m over that period. As a next step in reproducing the characteristics of the time series, the effect of the major tidal component was reproduced by using a free-stream velocity consisting of an oscillating flow superposed on the mean velocity field. Finally, to reproduce more accurately the time-dependent

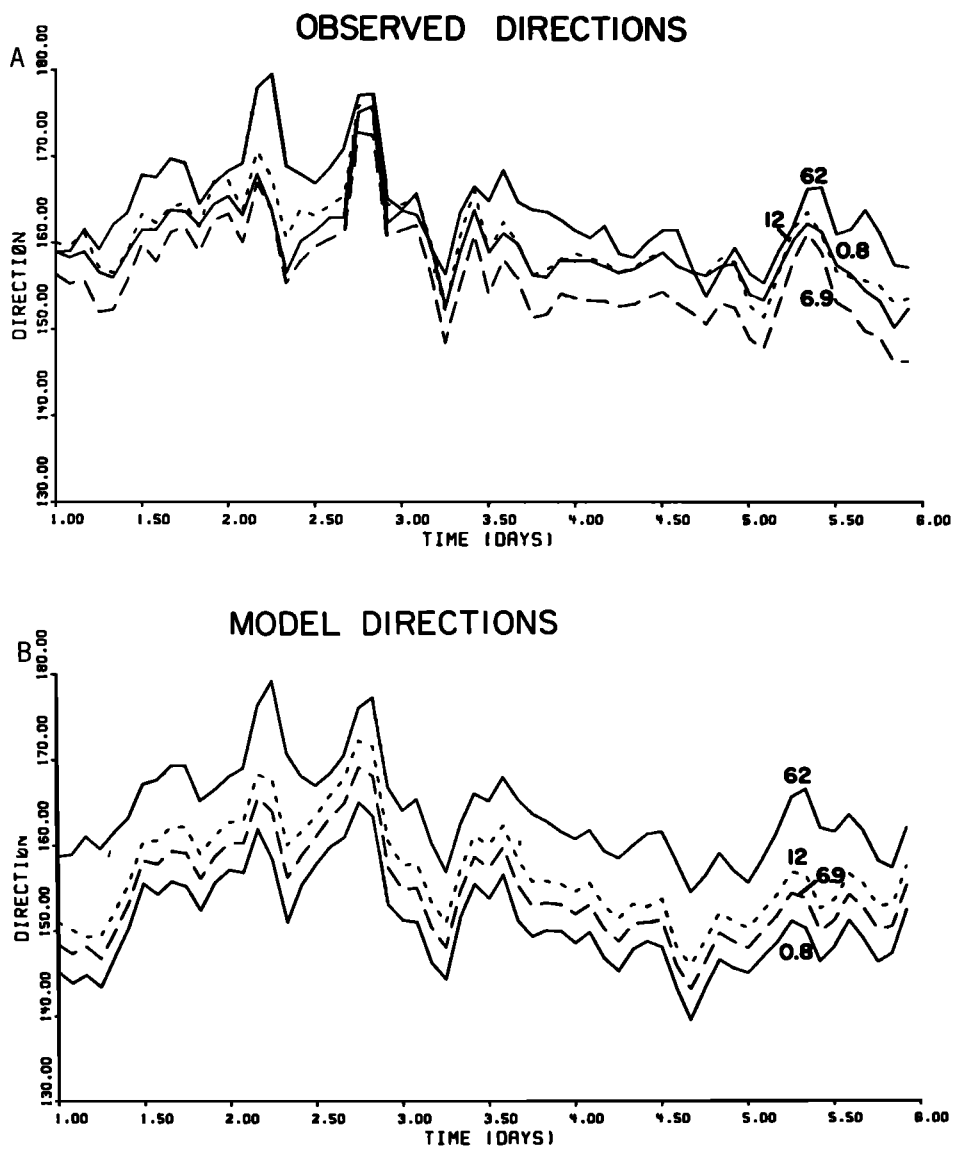

Fig. 8. (Top) Observed directions and (bottom) model direction predictions.

nature of the time series, the velocity measured at 62 m above the bottom was used as input for the model free-stream velocity. In all runs, the free-stream velocity was linearly increased to its starting value over 1 day to lessen the inertial oscillations associated with initializing the model.

Table 3*a* summarizes speed and direction relative to V_I at the four heights closest to the current meter positions for the three steady model simulations and for the 5-day averaged data. In the $\alpha = 0$, the bottom parallel isopycnal case, the speed at every level in the BBL is higher than the observed speed. In the $\alpha \neq 0$ simulations, the speeds at all levels in the BBL are reduced in comparison to the $\alpha = 0$ case. The profile for the observed speed averaged over the 5-day period (Figure 10) was drawn assuming a BBL thickness of 40 m as indicated by calculations using equations (5) and (7).

Hodographs using the mean observed and the simulated velocity components for the parallel and sloping isopycnal cases are depicted in Figure 11. A coordinate system was chosen such that the interior velocity has no u component for comparison to the model. The angle that the hodograph makes in the lowest part of the BBL represents the total veering angle, or total rotation of the current vector with depth. The veering predicted by the model is greater than that observed. The error in direction for the VACM is 2.0° [*Bryden*, 1976], so that the total error in the veering angle between any two current meters is at most 4.0°. Thus, the discrepancy between the data and the model results is significant. Table 3*b* summarizes the magnitude and direction of the bottom stress, friction velocity, total veering angle, and the thickness of the BBL. Inclusion of a slope in the model between the isopycnals and the bottom reduces the magnitude of the bottom stress and the friction velocity in comparison to the $\alpha = 0$ simulation. The bottom stress was computed from the 5-day averaged velocity observations as described in section 3. In the model, all of the terms in equation (8) are computed; that is, the time-dependent and slope terms are not neglected. The time-dependent terms are small (~10% of $|\vec{\tau_0}|$). The slope term calculated by the model is larger (~17% of $|\vec{\tau_0}|$ for a slope of 0.01 after $1\frac{1}{2}$ days, 39% after $2\frac{1}{2}$ days) and has the effect of decreasing the x component of the stress. Thus, as discussed earlier, if this term could be calculated from the data, the bottom stress might

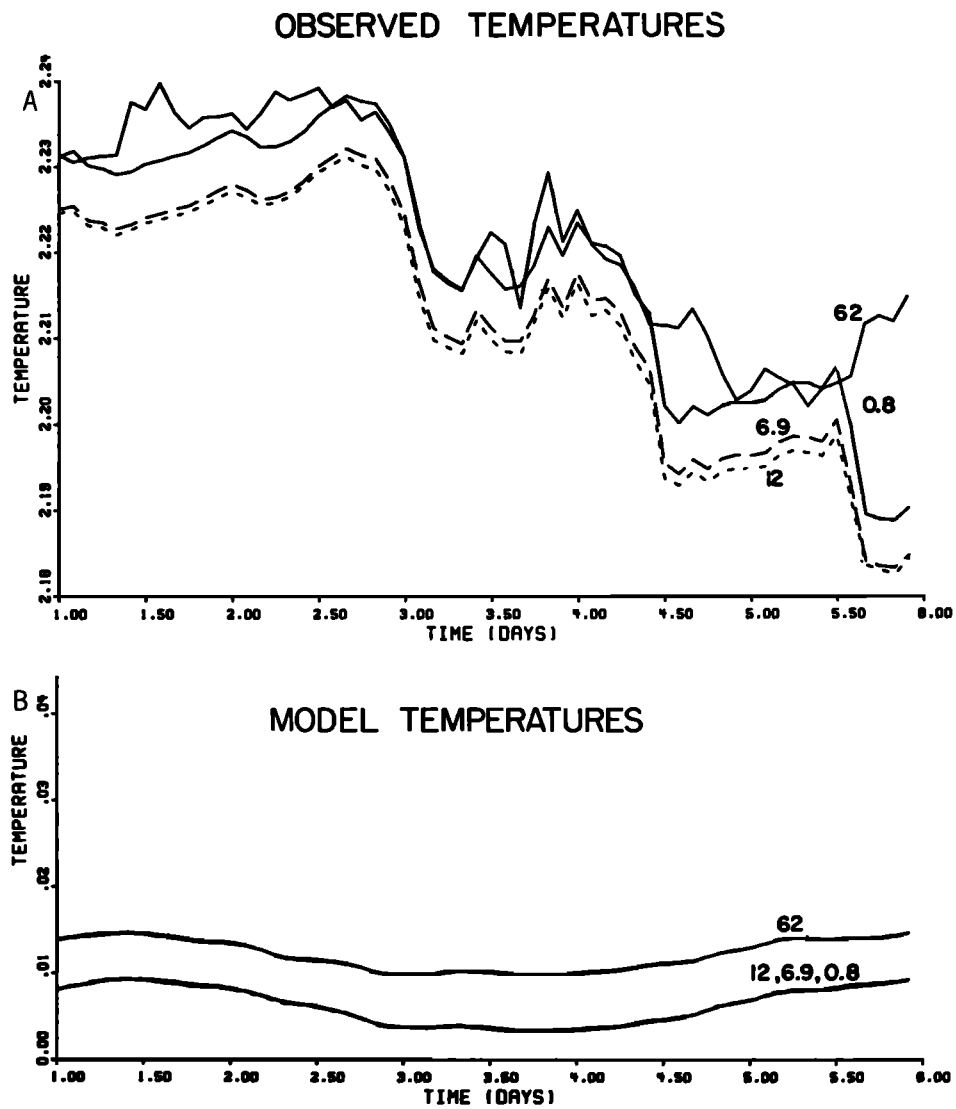

Fig. 9. (Top) Observed temperatures and (bottom) model temperature predictions.

agree more closely with the model bottom stress, particularly in direction.

To estimate the accuracy of the method used to calculate the bottom stress from the velocity data, the method was tested on model predictions treated as data. Vertical integration through the boundary layer using the trapezoidal rule and model velocities gives $\vec{\tau_0} = 0.50$ dynes/cm^2 directed at an angle 15.7 from $\vec{V}_1$, while the model predicts a stress of 0.47 dynes/cm^2 13.0° counterclockwise from $\vec{V}_1$. The error caused by making estimates with only four current meters may be calculated by using the four corresponding model velocities, yielding $|\vec{\tau_0}| = 0.66$ dynes/cm^2 and $\alpha_0 = 31.6°$. This is a 30% increase in magnitude and a 16.1° increase in angle. Thus, a large error in estimating $\vec{\tau_0}$ is due to having only four current meters. If nine current meters were used about 2 m apart in the vertical, this method would yield an estimate of $|\vec{\tau_0}|$ of

TABLE 3a. Mean Speeds and Directions for Days 1–5 of the Data and Three Model Simulations

	Data		Model					
			Slope = 0		Slope = 0.01		Slope = 0.035	
z (m)	Speed (cm/s)	Direc-tion	Speed (cm/s)	Direc-tion	Speed (cm/s)	Direc-tion	Speed (cm/s)	Direc-tion
62	18.92	0.00°	18.92	0.00°	18.92	0.00°	18.92	0.00°
12	17.87	3.30°	18.82	6.84°	18.68	6.46°	16.82	3.95°
6.9	16.61	7.57°	17.58	9.53°	17.45	9.03°	15.90	5.49°
0.8	11.93	4.04°	13.49	12.98°	13.39	12.47°	12.52	8.22°

A coordinate system was chosen such that there is no free-stream u-component of velocity for comparison of the data with model results. Directions are in degrees from $|V_1|$ and speeds are in cm/sec.

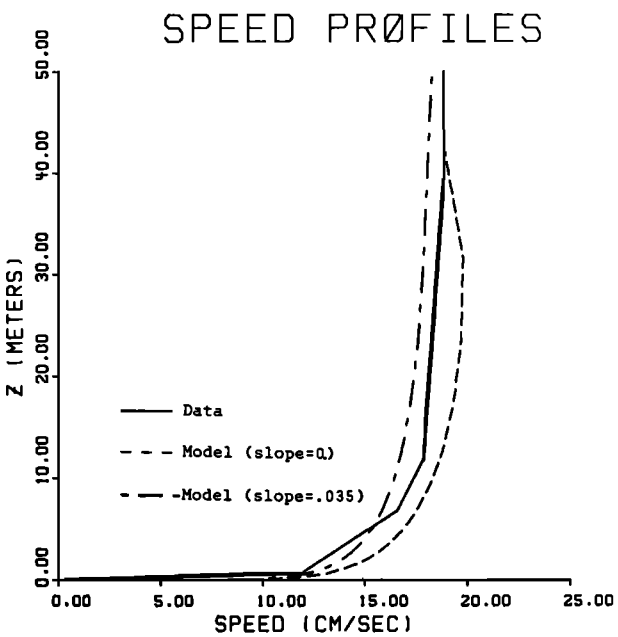

Fig. 10. Observed and model speed profiles. The model profiles were plotted from day 3 of the simulation. The data are average speeds over the 5-day period.

0.52 dynes/cm^2 at an angle of 26.8°, which is within 3% of the correct magnitude, and would substantially improve the estimates over those made with four current meters.

The error in the estimate of bottom stress contributed by the error in direction measured by the current meter can be estimated in this manner also. With only four current meters, an error of ±2° in any one current meter results in as much as a 13% change in magnitude and a 12% change in direction.

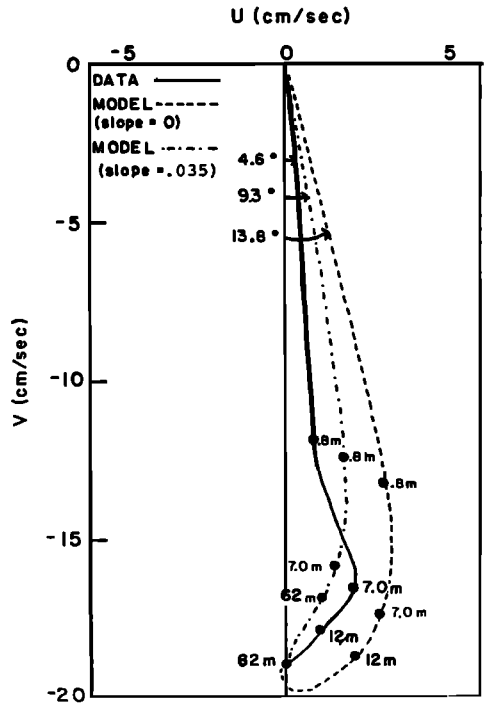

Fig. 11. Hodographs using velocity components at day 3 and the mean observed velocity components. The coordinate system was chosen such that the mean geostrophic velocity is directed along the negative y axis.

TABLE 3*b*. Magnitude of the Bottom Stress, Friction Velocity, Total Veering Angle, and Thickness of the Boundary Layer for the Observations and Three Model Simulations.

		Model		
	Data	Slope = 0	Slope = 0.01	Slope = 0.035
$\vec{\tau}_0$ (dynes/cm^2)	0.6	0.47	0.46	0.41
u_* (cm/s)	0.7	0.68	0.68	0.64
α_0 (degrees)	4.6	13.9	13.4	9.3
h (m)	41	36.7	36.7	90.4

In the model, h is resolved to $(^{+28\%}_{-22\%})$.

With nine meters, a 2° change in direction in any meter results in as much as a 9% change in magnitude of the stress and an 11% change in the direction. With four current meters, a change of 0.35 cm/s in speed, the error in speed measured by a VACM [*Bryden*, 1976], results in as much as a 3% change in the magnitude of the stress and as much as a 13% change in direction. With nine current meters, a 0.35 cm/s change in speed of any one current meter results in as much as a 2% change in the magnitude and a 10% change in the direction of the stress.

In the model the water column is initially linearly stratified. In the $\alpha = 0$ situation, as time progresses, the bottom layers become well mixed with a temperature equal to the average of the initial temperature at the top of the mixed layer and that at the bottom. Within 2–3 days a steady state is reached in the model with respect to all of the variables. However, a nonzero slope in the heat equation prohibits a steady temperature field from being attained. The model is formulated such that when the geostrophic current flows parallel to the isobaths with higher terrain to its right, the bottom slope is positive. As the bottom is approached in the BBL, the current vector rotates counterclockwise, giving the flow near the bottom a downslope component. If the isopycnal surfaces are level, the flow transports warmer water down the slope and the BBL continues to warm with time. After $1\frac{1}{2}$ days after a slope of 0.01 is introduced, the bottom mixed layer is 13 m thicker and 0.005°C warmer than in the $\alpha = 0$ case (Table 4).

Since in nature the BBL over a sloping bottom does not continue to warm indefinitely at a fixed point, the warming trend should be removed in the model and a steady state attained. First, a computer run is made with a nonzero slope and a mean velocity field whose free-stream velocity components are $(0, V_I)$. After several days of integration, the values of all the variables are stored for subsequent use as a 'basic state' and are denoted by the subscript 'BS.' The choice of the length of time of integration of the model determines only the actual temperature and thickness of the BBL: the longer the time, the warmer and thicker the mixed layer. Next, these basic state values are used to initialize the model in a new 'basic state' simulation. In the heat equation, the basic

TABLE 4. Progression of Model Variables in Time

	Day 2	Day 3	Day 4	Day 5
Bottom temperature (°C)	0.0030	0.0062	0.0090	0.0112
$\vec{\tau}_0$ (dynes/cm^2)	0.4654	0.4613	0.4660	0.4624
α_0	13.9°	13.4°	13.0°	12.7°
h (m)	36.7	36.7	49.6	49.6

The free-stream velocity was increased linearly from rest to 18.92 cm/s from day 0 to day 1. A slope of 0.01 was increased linearly from 0 between day 2 and day 2.5. In the model h is resolved to $(^{+28\%}_{-22\%})$.

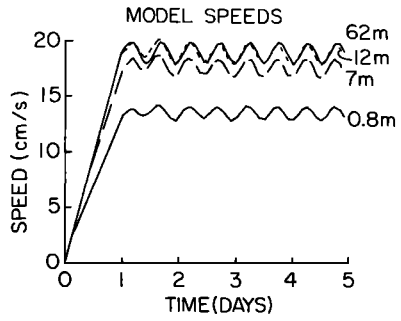

Fig. 12. Time series of speeds at 0.8, 7.0, 12, and 62 m predicted in a tidal simulation with $\alpha = 0$.

state U_{BS} is then subtracted from each ensuing U, and this difference is used in the equation, so that the temperature changes in time only if U is different from U_{BS}. Thus, for a steady velocity field (0, V_I) over a sloping bottom, the model reaches a steady state.

Physically choosing a 'basic state' after several days of integration is equivalent to saying that the boundary layer at the observational site was formed several days before. That is, water in the boundary layer at the site first encountered the bottom of the Eastward Scarp several days' time upstream.

To reproduce some of the time-dependent features of the data, the strongest tidal constituent was included in the model. A steady geostrophic current was increased linearly from rest to the mean value as before. Then, a rotary tidal current was added to the geostrophic velocity field. From rotary spectral analysis, the dominant tidal constituent at this location was the M_2 clockwise polarized component, with an amplitude of 1.35 cm/s and a frequency of 1.4×10^{-4} s^{-1} (Table 2):

$$V_I' = V_I - \text{amp} \sin(\omega t),$$

$$U_I' = \text{amp} \cos(\omega t)$$

where V_I is the 5-day average speed at 62 m (18.9 cm/s, Table 3*a*) and where amp is the tidal amplitude (1.35 cm/s Table 2) and ω is the tidal frequency (1.4×10^{-4} s^{-1}). In this simulation, isopycnal slope relative to the bottom slope was set to zero in order to examine only the effects of the tide.

The oscillatory component of the flow was small relative to the mean flow at all levels, and the effects of the tide on the flow were small (Figure 12). The magnitude of the bottom stress averaged over a tidal cycle was slightly greater for the combined flow than for the steady flow because of increased dissipation by the tidal flow. The bottom stress due to the M_2 clockwise polarized tide alone was 0.0038 dynes/cm^2 in magnitude, that due to the mean flow was 0.4689 dynes/cm^2, and that of the combined flow, averaged over a tidal period, was 0.4708 dynes/cm^2. In this case, the model shows that the tidal amplitude is too small to alter the flow parameters significantly.

To test fully the agreement between model and the data, measured values of the interior velocity can be used as input for the model in place of a steady geostrophic velocity or a combined steady tidal current. Although the VACM recorded an average velocity every 7.5 min, the study of *Weatherly and Wimbush* [1980] suggest that an appropriate Reynolds averaging interval for the BBL should be several hours. Thus, the 2-hour averaged velocity time series at 62 m was used as the interior velocity for the model, linearly interpolated into the 20-min time intervals required by the model. In the $\alpha \neq 0$ simulations, the basic state was taken to be the model output at the beginning of day 3 (Table 4); after day 3 the BBL thickness was too great.

The time series predicted by the model for speed and direction in the $\alpha = 0$ case are plotted in Figures 7*b* and 8*b*, and many observed features were reproduced by the simulation. For example, the observed speed at 12 m is higher than at 62 m at times 2.25–2.50 days and at 5.5 days, and this feature is reproduced in the simulation. Note that the predicted and observed records at 62 m should and do agree since the model BBL thickness is less than 62 m.

The fluctuations of the temperature time series were not reproduced by the model. Between 2.5 and 3.5 days the temperature decreased at all levels by 0.02° C (Figure 9*a*). In the $\alpha = 0$ simulations, the temperature remained constant in time. In the $\alpha = 0.01$ case, there was a decrease in temperature in the middle portion of the 5-day period, but not of the same magnitude as that observed. The cooling occurred during a period of relatively slow current speed and small veering angle, indicating that the mechanism that brings warmer water downslope was inhibited at that time due to a slowing of the free-stream flow.

The model temperature field responds to cross-stream advection but downstream advection is not modeled. The interior temperature fluctuations could be reproduced by using the 62-m temperature as the interior temperature. The BBL temperature field would fluctuate with the interior temperature. The observations indicate that the physics involved are more complex; for example, in Figure 9*a*, between 5.5 and 6.0 days, a drop of 0.2°C occurred in the temperature records at 0.8, 6.9, and 12 m, while a warming was felt at 62 m. Events of this nature cannot be reproduced by a one-dimensional model of the BBL.

5. Damping of Flow in the BBL

The Bermuda Rise measurements and output from the numerical model indicate that as the bottom is approached the semidiurnal tidal current is more damped in the BBL than the mean flow (Table 5). Unequal damping of tidal and steady flows has been observed in other BBL data sets [*Weatherly and Van Leer*, 1977; *Weatherly and Wimbush*, 1980]. This phenomenon is particularly evident in speed profile measurements made at the base of the Scotian Rise (40°06'N,62°29'W) in water depth of 4900 m. Savonius rotors located at heights of 0.7, 2.0, 3.9, 8.6, and 28.8 m above the bottom recorded speeds for 9 days in September 1979. Five-minute averages are plotted in Figure 13. Note that the flow exhibits turbulent behavior near the bottom becoming less turbulent higher in the BBL, implying a turbulent Ekman layer and justifying the use of a turbulence closure model.

TABLE 5. Percent Decrease in the Amplitude of the M_2 Clockwise Polarized Tide and in the Mean Current From 62 m in the Bermuda Rise Data and Model Simulation

	Data		Model	
	M_2+	Steady	M_2+	Steady
12 m	11	7	8	1
6.9m	15	12	19	7
0.8 m	45	37	38	29

Plus denotes clockwise polarization.

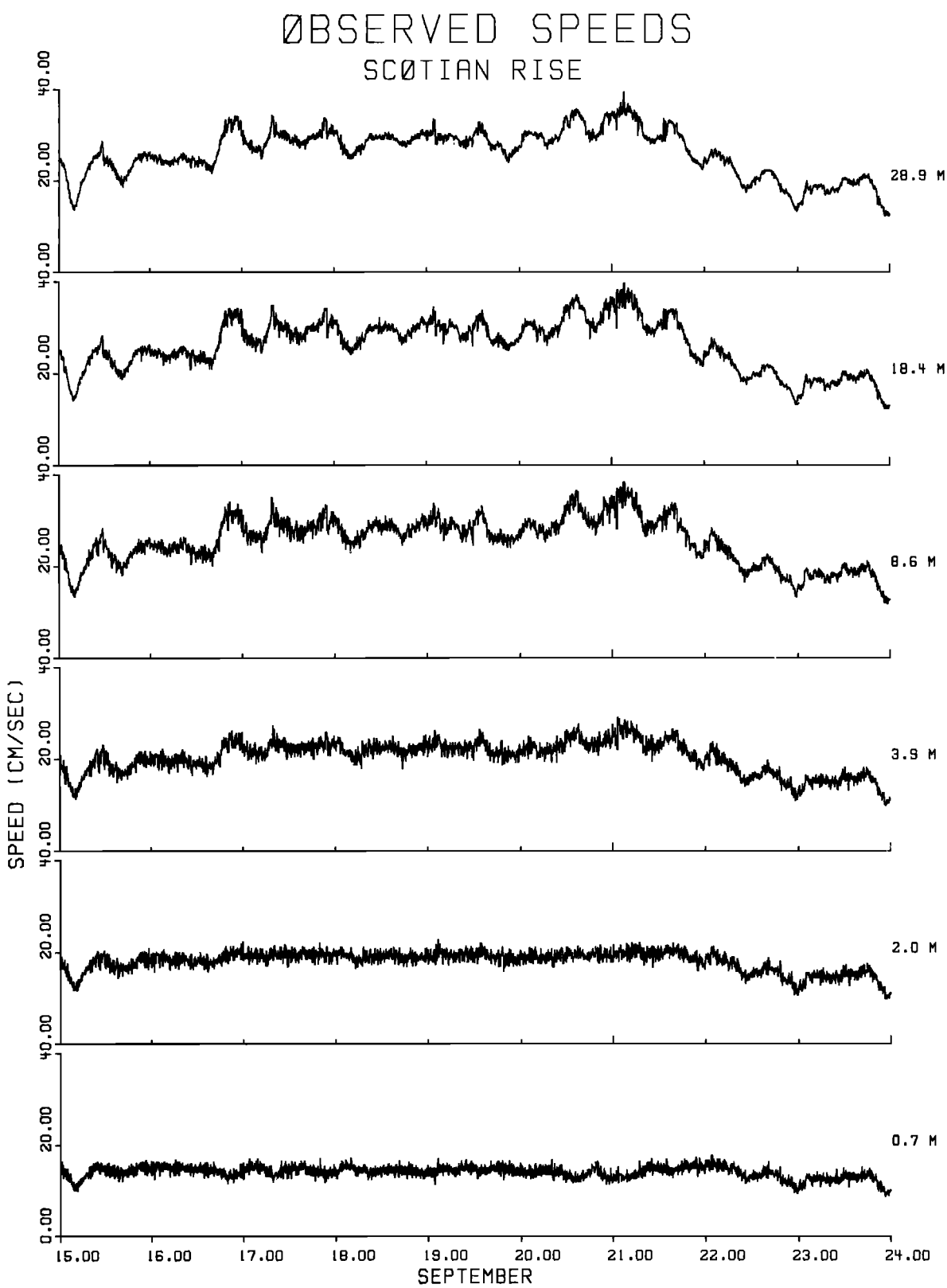

Fig. 13. Nine days of 5-min averaged speeds recorded at indicated heights above the bottom at the base of the Scotian Rise in water depth 4900 m.

Figure 14 depicts the same data, now averaged over 1-hour intervals. The semidiurnal tide is evident; rotary spectral analysis of currents in this region shows that this tidal component was primarily clockwise polarized. The amplitude of the tidal oscillations, which was about 8% of the mean speed at 28.8 m, decreased 60% to 0.7 m, while the mean current decreased only 45% between the same heights.

To determine whether this phenomenon is consistent with

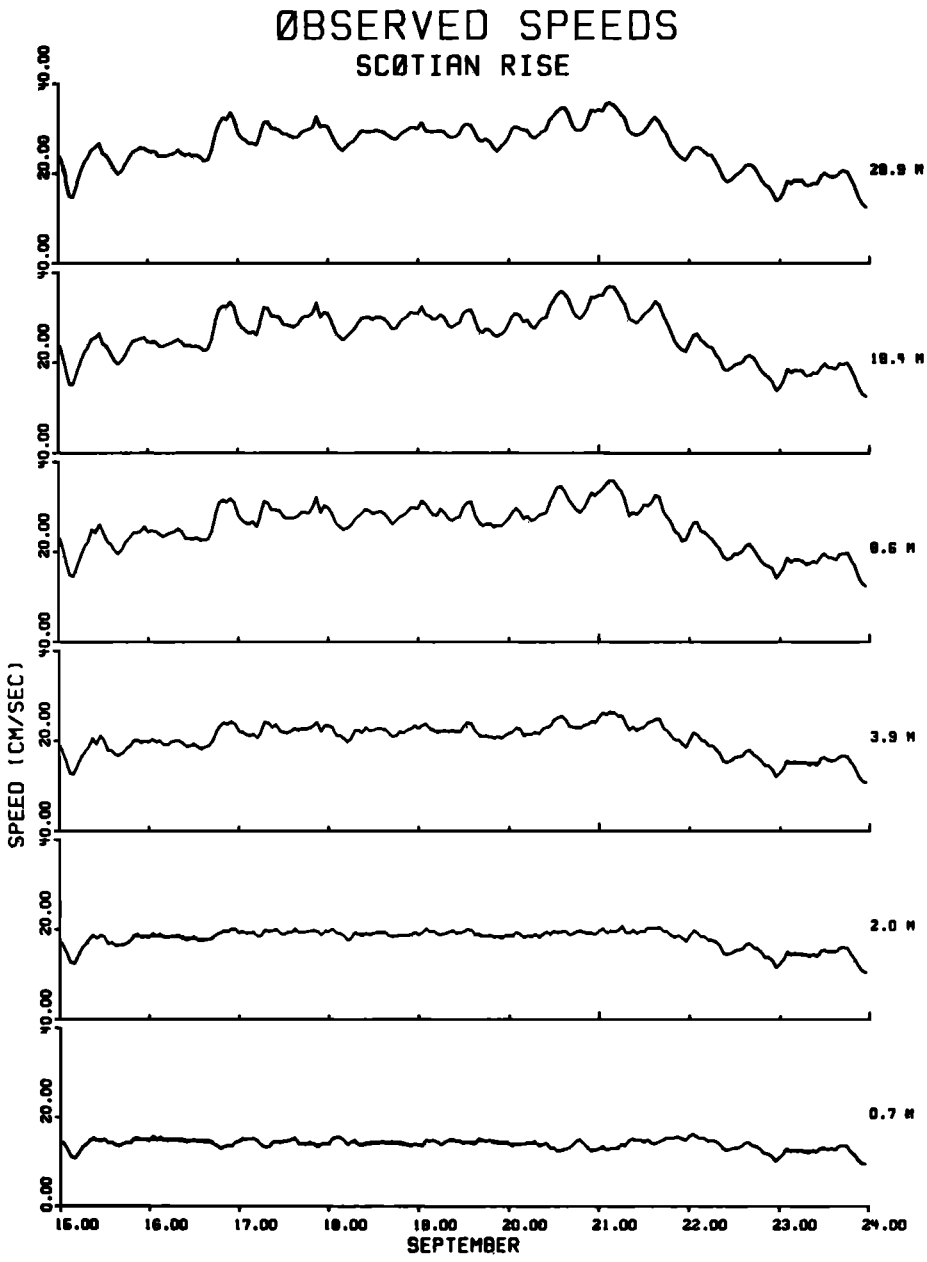

Fig. 14. As in Figure 13 except hourly averaged speeds.

boundary layer theory, a model simulation was made. As in previous simulations, the interior speed was ramped to the mean speed of 25.0 cm/s and then an M_2 clockwise polarized tide with an amplitude of 2.0 cm/s was superposed on the mean flow. Model output is plotted in Figure 15 at grid points closest to the rotor heights. The model reproduced the relative damping of the clockwise M_2 tide; the amplitude of the tidal oscillations decreased 55% from its interior value, while the speed of the steady current decreased only 44% from its geostrophic value. Table 6 summarizes the strengths of the tidal and mean flows relative to their values at 28.8 m above the bottom. Not only was the total damping greater for the tidal component, but also this damping occurred higher in the BBL. This feature is apparent in both the model output and observations.

Since the model predicts the damping of the tide relative to the mean flow in the BBL, the phenomenon must have its basis in some aspect of boundary layer dynamics. The thickness of an Ekman layer is proportional to $(A/\hat{f})^{1/2}$ where A is the effective eddy viscosity and $\hat{f}$ is the appropriate rate of rotation: f for steady flow, $\omega - f$ for clockwise polarized flow, and $\omega + f$ for counterclockwise polarized flow. In this case, A is determined primarily by the steady flow since the steady flow is much stronger than the tidal flow. At the latitude of the Scotian Rise, the ratio of the height of the Ekman layer for the M_2 clockwise polarized flow to the height for the steady flow is

$$\frac{[A/(\omega - f)]^{1/2}}{[A/f]^{1/2}} = [f/(\omega - f)]^{1/2} = 1.4$$

thus, the damping of the tidal signal relative to the mean flow can be explained in terms of Ekman layer thicknesses; the tide feels the effects of bottom friction higher in the water column than does the mean current.

At the latitude of the measurements over the Bermuda Rise, the ratio of the boundary layer height for the M_2 clockwise polarized tidal component to the height for the mean flow is 1.1, so that the unequal damping observed in the Scotian Rise measurements is not expected to be as pronounced in the Bermuda Rise data. Table 5 compares the damping of the M_2 clockwise polarized component and the steady flow for both the tidal model simulation and observations. The amplitudes of the major tidal components are known from rotary spectral analysis of the data (Table 2); this information may be used to test the theory further. Percent decrease in amplitude of each component of the flow from the value at 62.0 m is tabulated in Table 7, as well as the appropriate rotation rate and height relative to the height for the mean flow. The inertial motions and the K_1 and O_1 clockwise polarized tides have the thickest boundary layers and also show the most decrease in amplitude throughout the BBL. The counterclockwise polarized tides, having thin boundary layers associated with them, exhibit little damping until very close to the bottom. Thus the Bermuda Rise data substantially support this mechanism which explains the damping observed in the Scotian Rise data.

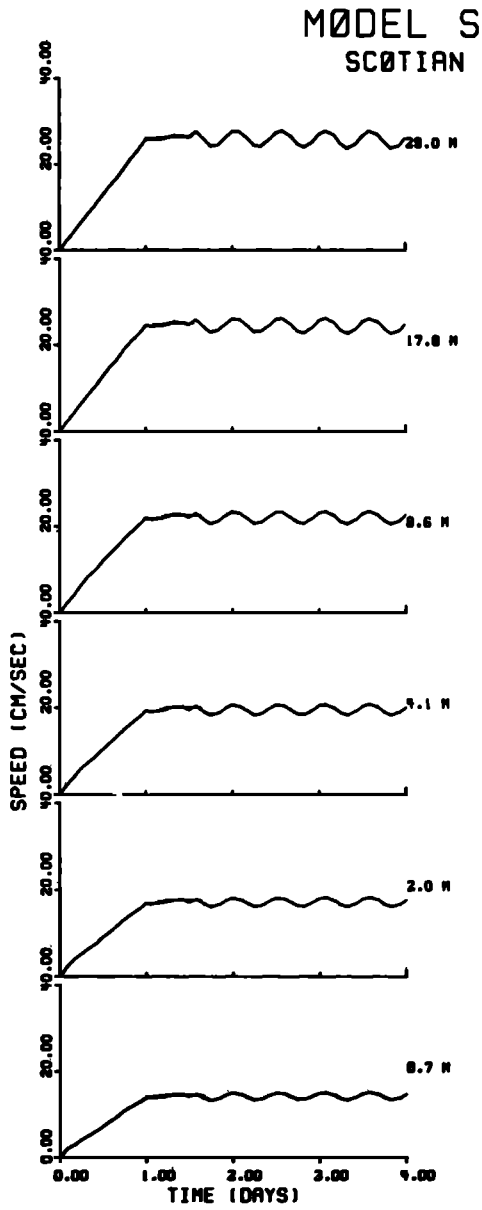

Fig. 15. Model speed time series for Scotian Rise at indicated heights above bottom.

TABLE 6. Percent Decrease in the Amplitude of the M_2 Clockwise Polarized Tide and in the Mean Current From 28.8 m From the Scotian Rise Data and Model Simulation

	Data		Model	
	M_2+	Steady	M_2+	Steady
18.4 m	0	0	10	5
8.6 m	10	2	25	15
3.9 m	30	22	35	25
2.0 m	40	30	45	33
0.7 m	60	45	55	44

Plus denotes clockwise polarization.

Discussion and Summary

We compared velocity and temperature measurements from a deep-ocean bottom boundary layer with the second-order turbulence closure BBL model of *Weatherly and Martin* [1978]. The thickness of the BBL, mean speed profiles, and the magnitude of the bottom stress compare favorably with the observations. The cross-stream component of the bottom stress τ_0^x estimated from the data by equation (8*a*) disagrees with model results due to the error in neglecting the term involving the isopycnal slope and due to the lack of data between the current meters at 12 and 62 m above the bottom. Future studies should sample temperature and velocity more densely throughout the BBL.

Two of the model's input parameters are not known precisely: the slope of the isopycnal relative to the bottom slope and the roughness parameter z_0. Simulations were made of the BBL with slopes of 0, 0.01, and 0.035. Inclusion of an isopycnal slope causes the speeds at all levels in the BBL to decrease and reduces veering angles. The friction velocity and bottom stress decrease slightly under sloping bottom conditions. The best agreement is attained using a slope of 0.01. A greater slope gives closer agreement by reducing the total veering angle, but the thickness of the BBL increases so much (h = 90 m 1 day after the addition of the slope) that the speed profiles no longer correspond as closely. Model results are not as sensitive to the choice of the roughness parameter. Decreasing z_0 results in a decrease in the total veering angle, giving better agreement with the data, but a smaller z_0 also means a smaller bottom stress and greater discrepancy with the data in that respect.

The discrepancy in veering angle between the data and the model is significant and cannot be attributed solely to instrumental error. One possible explanation for a reduced veering in the data lies in the topography. Furrows were found upstream of the mooring although none were found in the immediate vicinity [*McCave et al.*, 1982]. *Brown* [1970] solved the equation of motion to obtain helical rolls as finite perturbations on a mean large-scale flow in a boundary layer. In these solutions, the velocity profiles were altered so that the veering angle was reduced; velocity profiles made in the atmospheric boundary layer beneath parallel cloud lines give similarly reduced veering angles. Also, helical rolls result in reversed veering in the lower part of the boundary layer [*Brown*, 1980] and reverse (but not significant) veering is seen between 6.9 and 0.8 m in Figure 6. Furrows can set

TABLE 7. Percent Decrease From 62.0 m, Rotation Rate, and Relative Thickness of the Boundary Layer.

	Steady	M_2+	Inertial and K_1 and O_1	M_2-	K_1 and O_1-
12 m	7	11	15	−1	8
6.9 m	12	15	19	4	8
0.8 m	37	45	45	37	40
$\hat{f}(\times 10^{+4}\ s^{-1})$	0.791	0.616	0.089	2.199	1.494
h_{tidal}/h_{steady}	1.0	1.1	3.0	0.6	0.7

Plus denotes clockwise polarization; minus, counterclockwise polarization.

up, or may be caused by, organized motions in the BBL dynamically similar to those observed in the atmosphere, and the small veering angles observed in this study may be a result of these rolls. A photograph of a furrow, taken elsewhere in the deep North Atlantic, is in *Weatherly and Wimbush* [1980].

In addition to comparing mean quantities, the versatility of the model allows accurate reproduction of the time-dependent nature of the flow. A first approximation was made by using a free-stream velocity field consisting of the major tidal component, the M_2 clockwise polarized tide, superposed on the steady flow. Still better agreement is reached by using the velocity time series as measured at 62.0 m above the bottom to drive the model. The time series generated at the heights of the current meters correspond well to the observed time series. The large temperature fluctuations in the time series are not adequately reproduced by the model and are therefore not caused by cross-stream advection.

Differential damping with depth in the BBL of different constituents of the flow has been observed in the Bermuda Rise data and in speed measurements from the Scotian Rise BBL. In the free stream the amplitude of the M_2 clockwise polarized tide was 6% of the mean speed on the Bermuda Rise and 8% of the mean speed on the Scotian Rise. Model simulations with a steady flow plus a relatively small clockwise M_2 tidal current also show differential damping. The thickness of the Ekman layer due to a constituent of the flow depends uniquely on the effective eddy diffusivity and on the effective rotation rate. The former is determined primarily by the steady flow since the tidal amplitude is small relative to the mean speed, and the latter is determined by the latitude and by the frequency and polarization of the tide. The components of the flow that have thicker boundary layers associated with them feel the effects of bottom friction higher in the water column than do those associated with thinner boundary layers. Thus, different components of the flow are damped unequally in the BBL as the bottom is approached.

Acknowledgments. We thank W. Sturges, S. Blumsack, and W. Burnett for helpful suggestions to an earlier version of this work. L. Mayer is thanked for doing the rotary spectral analysis and M. Richardson for providing us with deep-tow CTD profiles. The assistance of R. Harkema and L. Vansant with programing and drafting is gratefully acknowledged. The Scotian Rise data were obtained as part of the HEBBLE program by D. Hunley. This research was sponsored by the Office of Naval Research under contracts N000-14-75-C-0201 and N000-14-76-C-0226.

REFERENCES

Bird, A. A., A study of the bottom boundary layer over the Eastward Scamp of the Bermuda Rise, M.S. Thesis, Florida State Univ., Tallahassee, 1981.

Blackadar, A. D., and H. Tennekes, Asymptotic similarity in neutral barotropic planetary boundary layers, *J. Atmos. Sci., 25,* 1015–1020, 1968.

Bowden, D. F., Physical problems of the benthic boundary layer, *Geophys. Surv., 3,* 255–296, 1978.

Brown, R. A., A secondary flow model for the planetary boundary layer, *J. Atmos. Sci., 27,* 742–757, 1970.

Brown, R. A., Longitudinal instabilities and secondary flows in the planetary boundary layer: A review, *Rev. Geophys. Space Phys., 18,* 683–697, 1980.

Bryden, H. L., Horizontal advection of temperature for low-frequency motions, *Deep Sea Res., 23,* 1165–1174, 1967.

Caldwell, D. R., C. W. Van Atta, and K. N. Helland, A laboratory study of the turbulent Ekman layer, *Geophys. Fluid Dyn., 3,* 125–160, 1972.

Csanady, G. T., On the resistance law of a turbulent Ekman layer, *J. Atmos. Sci., 24,* 467–471, 1967.

Hayes, S. P., The bottom boundary layer in the eastern tropical Pacific, *J. Phys. Oceanogr., 10,* 315–329, 1980.

Kundu, P. K., Ekman veering observed near the ocean bottom, *J. Phys. Oceanogr., 6,* 238–242, 1976.

McCave, I. N., E. P. Laine, P. F. Lonsdale, C. D. Hollister, and M. J. Richardson, Erosion and deposition on the eastern margin of the Bermuda Rise in the late Quaternary, *Deep Sea Res., 29,* 536–562, 1982.

Mellor, G. L., and T. Yamada, A hierarchy of turbulence closure models for planetary boundary layers, *J. Atmos. Sci., 31,* 1791–1806, 1974.

Mercado, A., and J. Van Leer, Near bottom velocity and temperature profiles observed by cyclosonde, *Geophys. Res. Lett., 3,* 633–636, 1976.

Schmitz, W. J., Jr., Weakly depth-dependent segments of the North Atlantic circulation, *J. Mar. Res., 38,* 111–133, 1980.

Weatherly, G. L., A study of the bottom boundary layer of the Florida Current *J. Phys. Oceanogr., 2,* 54–72, 1972.

Weatherly, G. L., and P. J. Martin, On the structure and dynamics of the oceanic bottom boundary layer, *J. Phys. Oceanogr., 8,* 557–570, 1978.

Weatherly, G. L., and J. Van Leer, On the importance of stable stratification to the structure of the bottom boundary layer on the western Florida shelf, in *Bottom Turbulence,* edited by J. Nihoul, pp. 103–122, Elsevier, New York, 1977.

Weatherly, G. L., and M. Wimbush, Near-bottom speed and temperature observations on the Blake-Bahama Outer Ridge, *J. Geophys. Res., 85,* 3971–3981, 1980.

Weatherly, G. L., S. L. Blumsack, and A. A. Bird, On the effect of diurnal tidal currents in determining the thickness of the turbulent Ekman bottom boundary layer, *J. Phys. Oceanogr., 10,* 297–300, 1980.

Worthington, L. V., and W. G. Metcalf, The relationship between potential temperature and salinity in deep Atlantic water, *Rapp. Cons. Explor. Mer,* 149, 122–128, 1961.

(Received February 4, 1982;
revised April 26, 1982;
accepted April 28, 1982.)